catalysts

MDPI

Article

Ru-(Mn-M)O_X Solid Base Catalysts for the Upgrading of Xylitol to Glycols in Water

Maxime Rivière [1], Noémie Perret [1], Damien Delcroix [2], Amandine Cabiac [2], Catherine Pinel [1] and Michèle Besson [1,*]

[1] Institut de recherches sur la catalyse et l'environnement de Lyon, University of Lyon, Univ. Claude Bernard Lyon 1, CNRS, IRCELYON, UMR5256, 2 Avenue Albert Einstein, 69626 Villeurbanne, France; mriviere@outlook.fr (M.R.); noemie.perret@ircelyon.univ-lyon1.fr (N.P.); catherine.pinel@ircelyon.univ-lyon1.fr (C.P.)

[2] IFP Energies Nouvelles, Rond-Point de l'Echangeur de Solaize, BP 3, 69360 Solaize, France; damien.delcroix@ifpen.fr (D.D.); amandine.cabiac@ifpen.fr (A.C.)

* Correspondence: michele.besson@ircelyon.univ-lyon1.fr; Tel.: +33-(0)472-445-358

Received: 26 July 2018; Accepted: 11 August 2018; Published: 14 August 2018

Abstract: A series of Ru-(Mn-M)O_X catalysts (M: Al, Ti, Zr, Zn) prepared by co-precipitation were investigated in the hydrogenolysis of xylitol in water to ethylene glycol, propylene glycol and glycerol at 200 °C and 60 bar of H_2. The catalyst promoted with Al, Ru-(Mn-Al)O_X, showed superior activity (57 h^{-1}) and a high global selectivity to glycols and glycerol of 58% at 80% xylitol conversion. In comparison, the catalyst prepared by loading Ru on (Mn-Al)O_X, Ru/(Mn-Al)O_X was more active (111 h^{-1}) but less selective (37%) than Ru-(Mn-Al)O_X. Characterization of these catalysts by XRD, BET, CO_2-TPD, NH_3-TPD and TEM showed that Ru/(Mn-Al)O_X contained highly dispersed and uniformly distributed Ru particles and fewer basic sites, which favored decarbonylation, epimerization and cascade decarbonylation reactions instead of retro-aldol reactions producing glycols. The hydrothermal stability of Ru-(Mn-Al)O_X was improved by decreasing the xylitol/catalyst ratio, which decreased the formation of carboxylic acids and enabled recycling of the catalyst, with a very low deactivation.

Keywords: hydrogenolysis; ethylene glycol; propylene glycol; xylitol; solid base catalyst; aqueous phase; alditol

1. Introduction

Ethylene glycol (EG) and propylene glycol (PG) are employed as raw or starting materials in various useful industrial applications, such as heat-transfer fluids and cosmetics, in the pharmaceutics and packaging sectors [1,2]. The global production of these glycols is currently based on the hydration of petroleum-based ethylene and propylene via epoxides intermediates [3], with 25 million metric tons being produced in 2017. Given recent strategies to diversify carbon sources, the use of bio-alditols, including xylitol and sorbitol, which can be obtained from inedible cellulose and hemicelluloses, appears to be a promising complementary process. Indeed, there are several advantages including the high C/O molar ratio of carbohydrates, the smaller environmental footprint, and their abundance [4–6].

In the last few decades, it has been reported that the upgrading of alditols to glycols can be performed in the aqueous phase under harsh conditions with temperatures of 160–230 °C and H_2 pressure (40–120 bar). The selective hydrogenolysis is challenging since parallel and consecutive reactions can occur and lead to a complex mixture of products [7–10]. The initial dehydrogenation of xylitol leads to an aldose (preferential route) or a ketose (minor route), according to the different rates of dehydrogenation of the primary or secondary hydroxyl groups. Then, C–C cleavage forms C_3

and C_2 intermediates by the retro-aldol reaction of the aldose or ketose catalyzed by base promotors, such as $Ca(OH)_2$. They are then hydrogenated to glycols or glycerol. Therefore, the (de)hydrogenation reaction is catalyzed by a heterogeneous metal-based catalyst and the retro-aldol step by an alkaline base. The decarbonylation reaction may also be catalyzed by the metallic sites and forms C_4 alditols (i.e., threitol) which can lead to the formation of butanediols (BDO) and CO via dehydroxylation and chain decarbonylation reactions [11]. In parallel, the epimerization reaction of xylitol produces other C_5 alditols (arabitol and adonitol) on metallic sites [12]. Moreover, lactate (LA) and 2-hydroxybutyrate (2-HBA) can be produced in the presence of a base by Cannizzaro-type reaction [9]. The main products observed in the hydrogenolysis of xylitol are reported in Figure 1. Thus, different strategies have been exploited in order to enhance the catalytic activity as well as glycols yield.

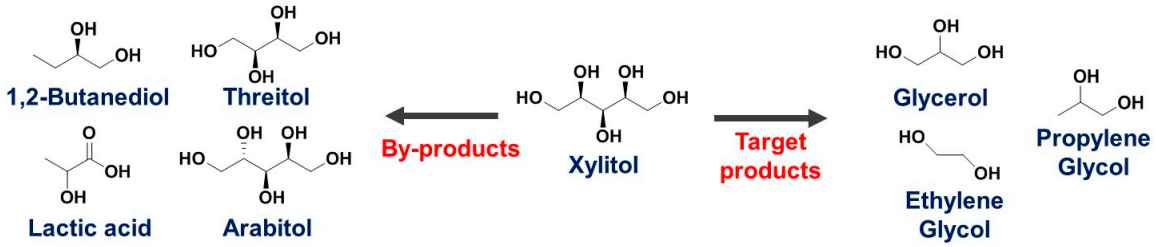

Figure 1. The main products observed during the hydrogenolysis reaction of xylitol.

Many metal-based catalysts, such as Cu, Ni, Ru, and Pt, have been studied for the hydrogenolysis of sugar alcohols to glycols, promoted or not by an alkali.

In the presence of $Ca(OH)_2$ base, 90%Cu-SiO_2 catalysts achieved glycols and glycerol yields of 50–60% in the aqueous phase at 200 °C under 60 bar of H_2. However, the catalytic activity was relatively low [13]. Ni-based catalysts, such as 6%Ni-NaY [14] and bimetallic 10%Ni-80%Cu-SiO_2 [15] catalysts displayed high selectivity to glycols and glycerol (up to 85%) at high conversion of the alditols in the presence of $Ca(OH)_2$. The Ru-based catalysts seem to be the most interesting candidates due to their high activity and their ageing resistance. Sun and Liu [9] reported a selectivity to glycols of 67% in the presence of 4%Ru/C catalyst in the hydrogenolysis of xylitol ($Ca(OH)_2$, 10 wt % xylitol in the aqueous phase, 200 °C and 40 bar H_2). Zhao et al. [16] observed a selectivity of 61% to glycols and glycerol over 3% Ru/carbon nanofibers. More recently, N-containing supports (amine-functionalized carbon nanotubes or covalent triazine framework) improved the performance of Ru-based catalysts in the presence of a base, in terms of activity [17] or yield of glycols and glycerol up to 85% [18].

Among strategies investigated to avoid both the addition of alkaline promoters and the formation of carboxylates, the use of bifunctional catalysts combining both metallic and basic sites has been studied. For instance, Ni-MgO catalysts [19] displayed a total selectivity to glycols and glycerol of 80% at 68% sorbitol conversion (in water, 200 °C, 40 bar H_2, 4 h). Some mixed oxide catalysts were also developed. Ni supported on fly ash (a waste mainly composed of SiO_2, Al_2O_3 and Fe_2O_3) showed a high global selectivity to glycols and glycerol (58% at 41% conversion) as well as high hydrothermal stability for four consecutive runs [20]. Catalysts supported on Ca-containing supports or directly on $Ca(OH)_2$ reached up to 60–70% selectivity to glycols at high conversion under base-free conditions. These include Cu-CaO-Al_2O_3 [21], Ni-Ru/$Ca(OH)_2$ (not stable because of the solubility of the support) [22], and more recently Ni-Ca(Sr)/hydroxyapatite catalysts [23]. Ni-Mg-Al-O hydrotalcite-like catalysts with different Mg/Al ratios were reported to be relatively stable during five runs with reasonable production of glycols [24]. In a previous study, we investigated the Mn promotion of a Ru/C catalyst for hydrogenolysis of xylitol in water [10]. We reported high activity (221 h^{-1}) and reasonable selectivity to glycols and glycerol (32%) over a 3%Ru/MnO(4.5%)/C catalyst. Moreover, we observed that the activity increased with the Mn-loading up to 384 h^{-1} and the selectivity to glycols and glycerol to 50% over 3.1%Ru/MnO(19.3%)/C catalyst. The selectivity over the same 3%Ru/MnO(4.5%)/C catalyst was then enhanced up to 70% in a water/alcohol mixture solvent, which

avoided the competitive decarbonylation reaction on the Ru sites [25]. Nevertheless, the catalyst had a poor hydrothermal stability.

Hereby, we developed promising mixed-oxide catalysts Ru-(Mn-M)O_X catalysts (M: Al, Ti, Zr, Zn) synthetized by co-precipitation, calcination and reduction. We compared different methods of Ru incorporation, which influenced the activity and the product distribution. Finally, we demonstrated that the Ru-(Mn-Al)O_X catalyst stability could be improved by varying the operating conditions.

2. Results and Discussion

2.1. Catalyst Characterization

The series of Ru-(Mn-M)O_X catalysts were obtained by thermal decomposition of co-precipitated precursors and reduction. For comparison, a Ru/(Mn-Al)O_X was prepared by impregnation of a Ru salt on (Mn-Al)O_X mixed oxide. The catalyst synthesis methods are reported in the Experimental Section. The M metal loading, the specific surface areas, the Ru crystallite sizes, and the number of acidic or basic sites are shown in Table 1. The loading of Ru could not be measured experimentally by ICP-OES, since Ru could not be totally solubilized, either in the solution of H_2SO_4 and HNO_3, or in concentrated HF solution. However, in the filtrate recovered after impregnation of Ru precursor, no traces of Ru were detected. The actual M loadings (i.e., Al, Ti, Zn, Zr) were very different from the nominal ones; in particular up to 97% of Al was lost (Table 1, entry 1). This might originate from the too high pH applied during the synthesis of the material, which is outside the limits of precipitation of aluminum hydrate and therefore alkaline dissolution of amorphous $Al(OH)_3$ to soluble sodium aluminate occurs. ICP-OES analysis of the solids after each synthesis step demonstrated that M loss took place during the filtration step; the M precursor had not been entirely precipitated despite the basic pH (12), the temperature (80 °C) and the ageing time (20 h). Meanwhile, whatever the method, the experimental Mn loadings were close to the nominal loadings.

Table 1. Characterization of the catalysts based on Ru, Mn and M: Al, Ti, Zr, Zn.

Entry	Catalysts	Nominal Loading [wt %]			Experimental Loading [1] [wt %]			Δ [2] [%]	S_{BET} [3] [m^2 g^{-1}]	Crystallite Size of Ru [4] [nm]	Total Number of Sites [μmol g^{-1}]	
		Ru	Mn	M	Ru	Mn	M				Basic [5]	Acid [6]
1	Ru/(Mn-Al)O_X	3	56	13	n.m.	66.5	0.5	97	13	6	28 (2.2)	18 (1.3)
2	Ru-(Mn-Al)O_X	3	70	4	n.m.	68.4	1.4	60	26	29	44 (1.7)	49 (1.8)
3	Ru-(Mn-Ti)O_X	3	64	11	n.m.	55.9	7.6	32	47	29	127 (2.7)	66 (1.4)
4	Ru-(Mn-Zr)O_X	3	60	15	n.m.	56.7	10.0	29	61	27	123 (2.0)	81 (1.3)
5	Ru-(Mn-Zn)O_X	3	60	15	n.m.	54.7	13.4	10	37	13	123 (3.3)	83 (2.2)

[1] Determined by ICP-OES, [2] Δ: loss of M during the synthesis, [3] relative error: ±5%; [4] based on Rietveld refinement, [5] determined by CO_2-TPD, [6] determined by NH_3-TPD; numbers in brackets represent the acid or basic site density [μmol m^{-2}]; n.m.: not measurable.

The specific surface area of the mixed-oxide catalysts varied in a large range from 13 to 61 m^2 g^{-1}. The catalyst where the Ru was deposited on the mixed-oxide (Ru/(Mn-Al)O_X, Table 1, entry 1) possessed a lower surface area than the catalyst where the Ru precursor was co-precipitated (Ru-(Mn-Al)O_X, Table 1 entry 2) with values of 13 and 26 m^2 g^{-1}, respectively. In the series of Ru-(Mn-M)O_X catalysts, the surface specific area varied as follows: Ru-(Mn-Al)O_X < Ru-(Mn-Zn)O_X- < Ru-Mn-Ti)O_X- < Ru-(Mn-Zr)O_X with 26, 37, 47 and 61 m^2 g^{-1}, respectively. These values are lower than those reported in the literature for dried or calcined Mn-Cu-Al layered double hydroxides [26]. The lowest specific area is associated with the lowest M content in the mixed oxide catalysts. This is not surprising, since MnO_X exhibits low surface area of 24 m^2 g^{-1} [10].

The XRD patterns of the Ru-(Mn-Al)O_X catalyst after each step of the synthesis highlighted the modification of the oxide species during the different thermal treatments, namely drying, calcination at 460 °C under air, and reduction at 450 °C under H_2 flow (Figure 2a). After drying, the only detectable crystalline phase was Mn_3O_4, whereas no peak corresponding to Al_2O_3 could be observed. The calcination step led to a mixture of Mn_3O_4 and Mn_5O_8, as reported in the literature under the

same atmosphere and similar temperature [27]. The Mn_3O_4 species consists of tetrahedral Mn(II) and octahedral Mn(III) units, which stem from partial oxidation of Mn(II) under hydrothermal conditions, as shown on the Pourbaix diagram [28,29]. The Mn_5O_8 species is a metastable oxide of equal amounts of Mn(II) and Mn(IV) [30]. Meanwhile, no peak corresponding to RuO_2 was observed, suggesting an amorphous phase or a small crystallite size (<2 nm). After reduction treatment, only peaks attributed to MnO were detected. Ru-(Mn-Zr)O_X, Ru-(Mn-Zn)O_X and Ru-(Mn-Ti)O_X samples presented similar patterns (Figure 2b). Furthermore, despite the high M amount in some of the catalysts, no peak attributed to the M oxide was observed, except ZnO in the Ru-(Mn-Zn)O_X material. This observation suggests that TiO_2 and ZrO_2 were amorphous, unlike in a Cu-ZrO_2-MgO material obtained after similar thermal treatment [31]. It is worth noting that the pattern of Ru-(Mn-Al)O_X recorded with a higher time per step (Figure A1) exhibited peaks associated with Mn_3O_4 in the 2θ region of 28–38°. This phase might also be present in the other Ru-(Mn-M)O_X. The Ru^0 crystallites were detected in all XRD patterns with different sizes depending on the synthesis method (Table 1). The Ru-(Mn-M)O_X catalysts prepared by co-precipitation exhibited higher Ru mean crystallite sizes (13–29 nm) than the catalyst prepared by deposition of Ru over the (Mn-Al)O_X support (Ru/(Mn-Al)O_X, 6 nm). This is probably due to the calcination step. As reported in the literature for 4%Ru/Al_2O_3 catalyst [32], small RuO_2 crystallite sizes (<2 nm) are formed upon calcination, however, sintering of Ru particles occurs during reduction. On the other hand, the Ru/(Mn-Al)O_X catalyst underwent the reduction step without the initial calcination step leading to a small mean crystallite size of Ru.

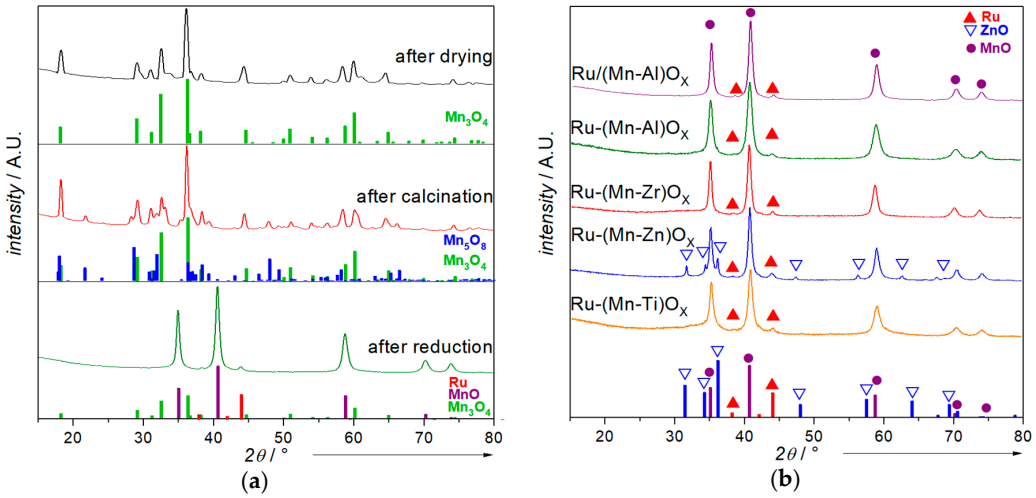

Figure 2. XRD patterns of: (**a**) Ru-(Mn-Al)O_X catalyst after the different thermal treatments; (**b**) Ru/(Mn-Al)O_X catalyst and Ru-(Mn-M)O_X catalysts (M: Al, Zr, Zn, Ti).

Morphology of Ru/(Mn-Al)O_X and Ru-(Mn-Al)O_X catalysts was analyzed by TEM. Images of Ru-(Mn-Al)O_X replica (Figure 3b) revealed a broad size distribution of large (50–100 nm) and small (<5 nm) Ru particles. The images of Ru/(Mn-Al)O_X replica (Figure 3a) showed a homogeneous size of small Ru particles (3–7 nm) gathered together as wormlike nanoparticles. These TEM observations are in accordance with the Ru crystallite size measured by XRD. Significant differences in the size and distribution of Ru particles may influence the activity and the product distribution in hydrogenolysis of xylitol.

The acid-base properties were investigated by CO_2 and NH_3 TPD. In the case of Al-containing materials, the result was dependent on the method of introduction of Ru. In CO_2-TPD profiles (Figure 4a), three main peaks at 175, 250 and 450 °C were detected and attributed to weak, moderate and strong basic sites, respectively. Ru/(Mn-Al)O_X catalyst contained mostly weak basic sites. The signal at 450 °C would be associated with CO_2 adsorbed on strong basic sites or on Ru particles, according to the literature [10,33]. The Ru-(Mn-M)O_X catalysts showed different desorption patterns that are a

function of the nature of M. Catalysts Ru-(Mn-M)O_X with M: Zr, Zn, or Ti contained a majority of weak and moderate basic sites due to the presence of possible ZrO_2, ZnO and TiO_2 phases [34,35]. Stronger basic sites were observed on Ru-(Mn-Al)O_X catalysts, which is likely due to the higher content of Mn in this material. The total number of basic sites (in μmol g^{-1}) was as follows: Ru/(Mn-Al)O_X (28) < Ru-(Mn-Al)O_X (44) < Ru-(Mn-Zr)O_X, Ru-(Mn-Zn)O_X (123) ≈ Ru-(Mn-Ti)O_X (127), while the basic site density (in μmol·m^{-2}) was as follows: Ru-(Mn-Al)O_X (1.7) < Ru-(Mn-Zr)O_X (2.0) < Ru/(Mn-Al)O_X (2.2) < Ru-(Mn-Ti)O_X (2.7) < Ru-(Mn-Zn)O_X (3.3) (Table 1). Since the M oxides have an amphoteric character, acid sites were also analyzed (Figure 4b). They are present in lower amounts than basic sites (18 to 83 μmol g^{-1}, i.e., acid density of 1.3–2.2 μmol m^{-2}).

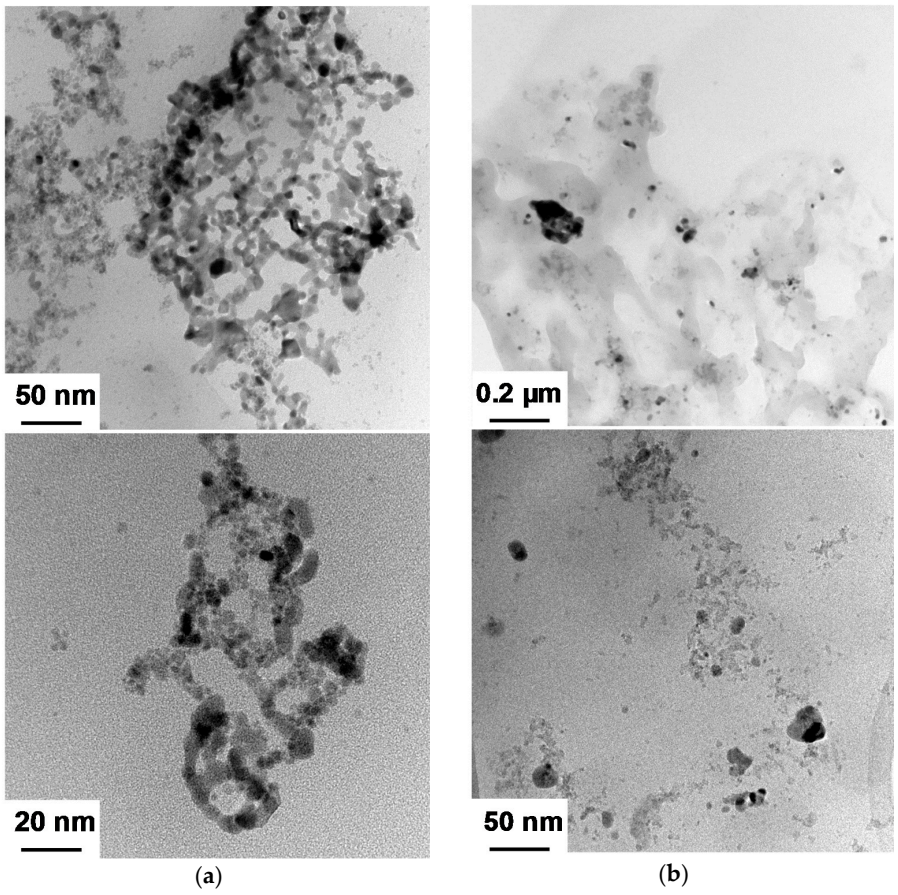

Figure 3. TEM images of replica: (**a**) Ru/(Mn-Al)O_X; (**b**) Ru-(Mn-Al)O_X catalysts.

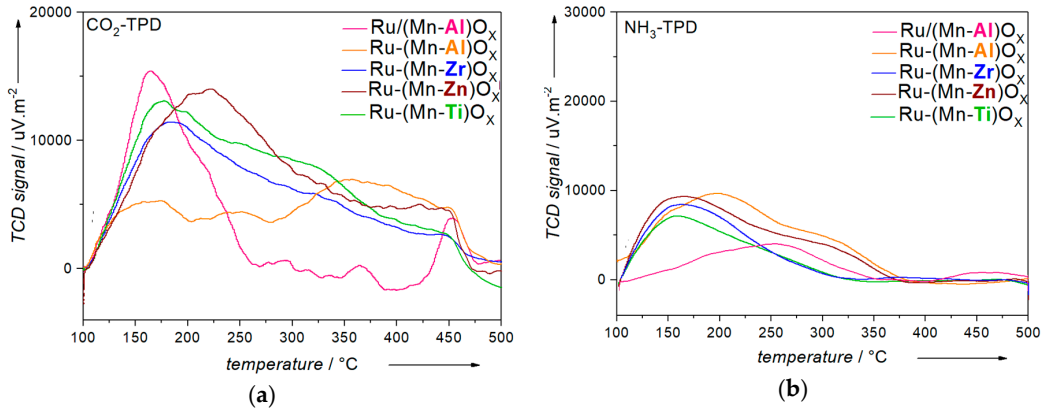

Figure 4. TPD profiles of mixed-oxide catalysts using as probe: (**a**) CO_2; (**b**) NH_3.

To summarize, the introduction of a M promoting element modified the specific surface area and total number of acid and basic sites, whereas the MnO_X phases (Mn_3O_4 and MnO) and the Ru crystallite size remained relatively the same. Meanwhile, the two methods of addition of Ru (via co-precipitation and deposition methods) showed that Ru/(Mn-Al)O_X contained small Ru particles, however, they were gathered while Ru-(Mn-Al)O_X contained small and large Ru particles with a heterogeneous distribution. These differences may influence considerably the catalytic performances in hydrogenolysis of xylitol.

2.2. Hydrogenolysis of Xylitol

The reactions were conducted in water at 200 °C and 60 bar H_2, without any alkali addition. The results of activity and selectivity to the main products are shown in Table 2. The selectivities are given at 80% conversion when the maximum concentration of the desired products was reached, as described previously [10,25]. The total carbon balance (comparison between TOC measured and TOC calculated from HPLC analysis) was around 90%.

Table 2. Activity and product distribution in the hydrogenolysis of xylitol over Ru-based mixed-oxide catalysts [1].

Catalyst	Activity [h^{-1}]	Carbon Selectivity [2] [%]							CB_T [4] [%]
		EG	PG	GLY	LA	C_4 Products [3]	C_5 Alditols	Gas Phase Products	
Ru/(Mn-Al)O_X	111	12	17	8	4	11	6	32	90
Ru-(Mn-Al)O_X	57	21	28	9	3	5	2	20	87
Ru-(Mn-Zr)O_X	33	21	29	9	2	5	3	23	92
Ru-(Mn-Ti)O_X	33	22	29	8	2	7	3	26	99
Ru-(Mn-Zn)O_X	0	-	-	-	-	-	-	-	-

[1] Conditions: xylitol 10 wt % (15 g), 135 mL H_2O, 0.5 g catalyst (molar ratio xylitol/Ru: 764), 60 bar H_2, 200 °C; [2] determined at 80% conversion; [3] C_4 products: threitol, erythritol, butanediols; [4] CB_T: Total carbon balance.

The catalytic performance depended on the mode of introduction of Ru in the Al-promoted materials. Indeed, the activity was halved from 111 h^{-1} for Ru/(Mn-Al)O_X to 57 h^{-1} for Ru-(Mn-Al)O_X. In parallel, the selectivities towards glycols were enhanced in the presence of Ru-(Mn-Al)O_X (21% to EG and 28% to PG) vs. Ru/(Mn-Al)O_X (12% to EG and 17% to PG). The selectivity to lactic acid (LA) and to glycerol (GLY) remained the same. On the contrary, the cumulated selectivity to C_4 and C_5 alditols decreased from 17% to 7%. Moreover, the products transferred into the gas phase (determined as the difference of initial TOC and TOC measured in the liquid phase) were produced in lower amounts over Ru-(Mn-Al)O_X. This observation suggests that the side reactions of cascade decarbonylation leading to the degradation of glycols, particularly EG, were minimized [25]. This was confirmed by the calculation of the molar ratio of C_3 to C_2 products, which was 1.3 and 1.9 for the reactions in the presence of Ru-(Mn-Al)O_X and Ru/(Mn-Al)O_X, respectively, while the theoretical molar ratio is 1.0 for a totally selective hydrogenolysis reaction of xylitol to EG plus PG. Therefore, the Ru-(Mn-Al)O_X catalyst favored the retro-aldol reaction instead of the decarbonylation reactions. In contrast, Ru/(Mn-Al)O_X contributed to the decarbonylation reactions. Since the latter reactions take place on Ru particles, the larger particle sizes of Ru-(Mn-Al)O_X (as shown by TEM and XRD) may explain why side-reactions observed at 80% xylitol conversion are not significant, in addition to showing lower activity. Otherwise, the presence of a higher number of basic sites on Ru-(Mn-Al)O_X than on Ru/(Mn-Al)O_X favors the retro-aldol reaction to the detriment of epimerization or cascade decarbonylation reactions, which explains the decrease in catalytic activity.

The Ru-(Mn-Zn)O_X material was not active at all and no conversion was measured after a reaction time of 30 h. A comparable result was observed in our previous study using Ru/ZnO/C catalyst; the catalytic activity decreased from 220 to 13 h^{-1} in comparison with Ru/MnO/C catalyst [25]. Yet, previous studies have reported that the combination of Cu and ZnO was active and selective in the

hydrogenolysis of alditols to glycols [21,36–38]. The activity of Ru-(Mn-Zr)O_X and Ru-(Mn-Ti)O_X catalysts was 33 h^{-1}, i.e., lower than the activity of Ru-(Mn-Al)O_X (57 h^{-1}). The product distribution was quite similar whatever the promoter. At 80% xylitol conversion, the cumulated selectivity to glycols and GLY was as high as 59% and the values of selectivity to C_4 and C_5 products were maintained in the range 7–10%. The selectivity to gaseous products increased slightly in the presence of Ru-(Mn-Zr)O_X and Ru-(Mn-Ti)O_X to 23% and 26%, respectively, vs. 20% over Ru-(Mn-Al)O_X catalyst. Thus, in general, despite the relatively high amount of M introduced (10 wt % Zr and 7.0 wt % Ti) and the various total number of acid and basic sites, the use of M promotor had no significant effect on the product distribution. This suggests that a low number of basic sites was sufficient to efficiently perform the retro-aldol reaction, whereas the acid sites favor the cascade decarbonylation to produce gaseous products. Moreover, the activity of Ru-(Mn-Al)O_X is higher due to the higher amount of Mn in the bulk. It has been previously shown that the amount of Mn introduced on the support before deposition of Ru accelerated the conversion of xylitol in base-free medium [10].

Compared to Ru-based catalysts described in the literature for hydrogenolysis of alditols in water under base-free conditions, the Ru-(Mn-Al)O_X catalyst is the most selective to glycols and GLY (58%). This selectivity was 41% from sorbitol over Ru/$Ca(OH)_2$ [22] and 32% from xylitol over Ru/MnO/C [10]. The selectivity of Ru-(Mn-Al)O_X is equal to that of a few Ni-based catalysts, such as Ni-(Mg-Al)O_X [24] or Ni/fly ash [20]. It is close to the one of the best catalytic systems, such as Ni-CaO/C [39] and Cu/CaO-Al_2O_3 [21], which displayed a selectivity to GLY and glycols of 69% and 73%, respectively; however, the latter Ni catalysts were less active in the hydrogenolysis under similar reaction conditions of alditols with values of 20 and 0.4 h^{-1} respectively, compared to Ru-(Mn-Al)O_X (57 h^{-1}).

The stability of the catalysts was investigated by analysis of the leaching of the catalyst in the final solution and of the used catalyst by XRD. No Ru leaching was observed (detection limit ICP-OES; <0.2 mg L^{-1}, <0.15 wt %), Zr and Ti leaching was less than 1 wt %, while 13–16 wt % of Al were leached. These observations are in line with the literature on the higher stability of TiO_2 and ZrO_2 than Al_2O_3 as support for Ru under hydrothermal conditions under H_2 atmosphere [40]. On the contrary, a Mn leaching as high as 42–48 wt % was observed for all catalysts. Although this value was still too high, the Mn leaching from Ru-(Mn-M)O_X catalysts was below the one from Ru/MnO/C of 63–70 wt % under the same reaction conditions [10]. The Mn leaching is associated with the production of carboxylic acids, such as lactic or 2-hydrobutyric acids, which were analyzed in the final reaction medium [10,33]. While Mn_3O_4 and MnO were observed in the fresh catalyst, only $MnCO_3$ was detected in the used catalyst. Similarly, calcium carbonate was detected over Ru/$Ca(OH)_2$ catalyst after hydrogenolysis of sorbitol under similar conditions [22].

2.3. Influence of Operating Conditions

The operating conditions (H_2 pressure, temperature) may have a significant influence on the product distribution, as shown over a Ru/C catalyst in hydrogenolysis of xylitol [9]. We investigated the H_2 pressure in order to decrease the carboxylic acids production and thus avoid the Mn leaching. Figure 5 shows the selectivity to the main products as a function of pressure over Ru-(Mn-Al)O_X catalyst.

An increase of H_2 pressure from 60 to 100 bar at 200 °C doubles the molar fraction of H_2 solubilized in aqueous solution [41]. However, catalytic activity increased only slightly from 52 to 59 h^{-1}, suggesting that the solubility of H_2 in water was not the limiting step. As for the product distribution, the cumulated selectivity to glycols decreased slightly from 48% to 43%. The selectivity to GLY increased gradually from 7% to 10%, and the selectivity to carboxylic acids (LA + 2–HBA) was reduced from 8.5% (7.5% LA; 1.0% 2–HBA) to 3.4% (2.7% LA; 0.7% 2–HBA). According to the scheme of the proposed reaction, GLY and LA come from the same intermediate, namely glyceraldehyde, via hydrogenation of the terminal carbonyl or via dehydration followed by Cannizzaro-like reaction; thereby, the pressure of H_2 favored GLY production at the expense of LA [9]. Nevertheless, despite the

decrease in carboxylic acid production, the crystalline phase of the catalyst at the end of the reaction was $MnCO_3$, and Mn leaching still occurred.

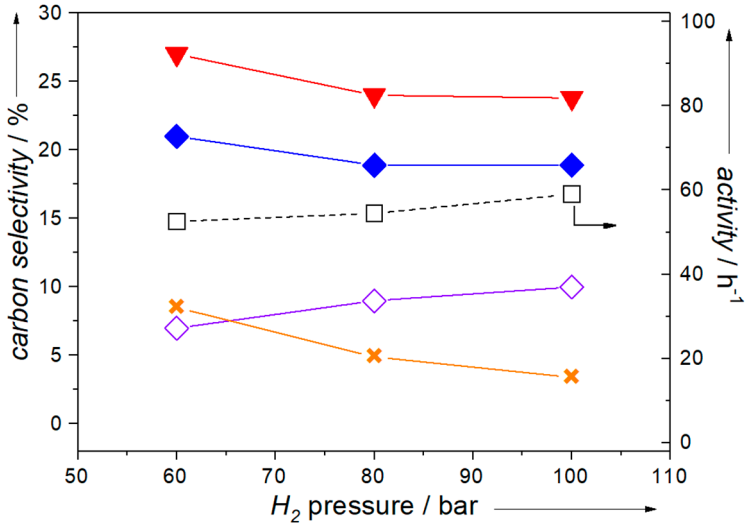

Figure 5. Influence of H_2 pressure on the activity and the selectivities to the main products in hydrogenolysis of xylitol in the presence of Ru-(Mn-Al)O_X. □ activity, ▼ PG, ◆ EG, × carboxylic acids (LA plus 2–HBA), ◇ GLY; Conditions: xylitol 10 wt % (15 g), 135 mL H_2O, 0.5 g Ru-(Mn-Al)O_X (molar ratio xylitol/Ru: 764), 60–100 bar H_2, 200 °C.

In addition, the substrate to catalyst ratio was investigated at 200 °C and 60 bar H_2 by modifying the amount of catalyst. The mass ratio was varied from 30 to 3, i.e., a molar xylitol/Ru ratio from 764 to 77. The activity, the product distribution, and the Mn leaching at the end of reaction are shown in Figure 6.

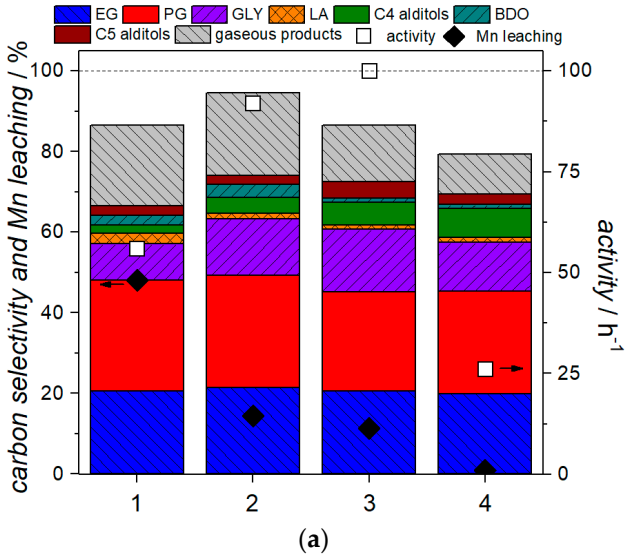

(**a**)

Reaction #	$m_{catalyst}$ [g]	$m_{xylitol}$ [g]	Molar Ratio $_{xylitol/Ru}$
1	0.5	15	764
2	1.0	15	383
3	1.5	15	255
4	0.5	1.5	77

(**b**)

Figure 6. (**a**) Influence of catalyst mass on the activity, selectivity, and Mn leaching: (**b**) Table of the operating parameters. Conditions: xylitol 1–10 wt % (1.5–15 g), 135 mL H_2O, 0.5–1.5 g Ru-(Mn-Al)O_X (molar ratio xylitol/Ru: 77–764), 60 bar H_2, 200 °C.

Normalized to the Ru moles, the catalytic activity increased from 57 h^{-1} to 101 h^{-1} as the catalyst mass increased (molar ratio from 764 to 255, Reaction #1–3), confirming that the Mn amount in the reaction system enhanced the activity, as observed in Table 2 and as reported previously [10]. When normalized to the total moles of Ru and Mn, the catalytic activity also varied by a factor of 2 between 1.1 and 2.0 mol_{xyl} $mol_{Ru+Mn}{}^{-1}$ h^{-1}. Assuming that Mn is responsible for the retro-aldol reaction and Ru for the (de)hydrogenation reactions, the difference in the catalyst activity suggests a pseudo-order reaction higher than 1 for the retro-aldol reaction. The product distribution was notably similar whatever the mass of catalyst: the cumulated selectivity to GLY and glycols remained in the range 57–60%, while the selectivity to C_5 and C_4 products was 10%; the selectivity to carboxylic acids decreased from 5% to less than 1% as the xylitol/catalyst ratio decreased. Surprisingly, Mn leaching at the end of reaction dropped from 48% to 10% as the xylitol/Ru molar ratio decreased from 764 to 255. Meanwhile, Al leaching decreased from 15% to less than 1%, and the Ru leaching remained below the detection limit. Therefore, in order to emphasize this effect, the xylitol/catalyst molar ratio was further decreased to 77, using a 1.0 wt % xylitol solution (Figure 6, Reaction #4). Activity decreased to 25 h^{-1} suggesting mass transfer limitations. Interestingly, Mn leaching was below 1%, i.e., 45 mg L^{-1} Mn in the final reaction medium.

Furthermore, XRD analysis of the used Ru-(Mn-Al)O_X catalyst (Figure 7) showed that the main crystalline phase was $MnCO_3$ after reactions using xylitol/Ru molar ratio between 764 and 255 (reactions #1–3). However, no peak attributed to $MnCO_3$ was detected in the used catalyst after reaction at molar ratio of 77 (reaction #4). Only peaks of Mn_3O_4 and large peaks of the hydrated MnO phase, $Mn(OH)_2$ were observed [42]. Therefore, the stability of Ru-(Mn-Al)O_X was enhanced by diminishing the xylitol/catalyst mass ratio (molar ratio 77), which made the recycling of the catalyst interesting.

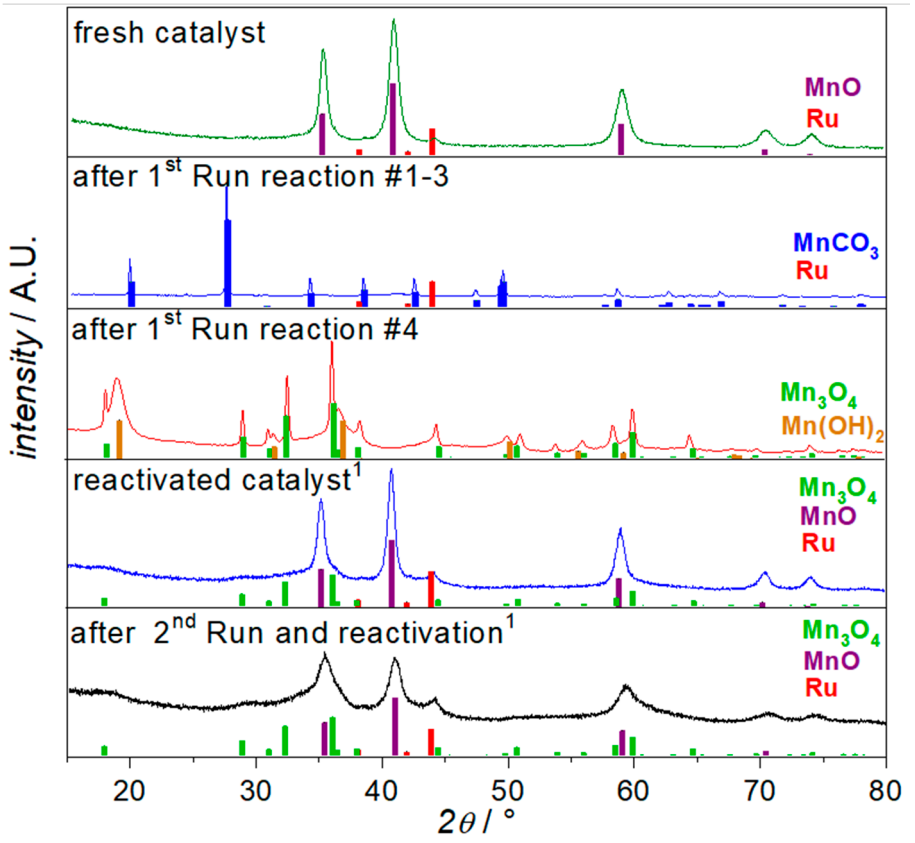

Figure 7. XRD patterns of catalyst Ru-(Mn-Al)O_X after reactions #1–4 and reactivation. [1] Reduction at 450 °C under H_2 flow for 3 h.

After the first run, the used Ru-(Mn-Al)O_X catalyst was washed with distillated water and reduced at 450 °C for 3 h in order to eliminate the surface hydroxyls and to reactivate Ru. The XRD analysis of the reactivated catalyst in Figure 7 shows that MnO was again the main crystalline phase. Small peaks associated with Mn_3O_4 can also be observed. It has been reported that formation of amorphous MnO_X and Mn_3O_4 phases leads to an increase of specific surface area [43]; this was observed with the reactivated catalyst whose specific area was enhanced from 28 to 60 $m^2\ g^{-1}$. These changes did not significantly modify the performance in hydrogenolysis of 1.0 wt % of xylitol in water with a molar ratio xylitol/Ru of 77, as shown in Table 3.

Table 3. Activity and product distribution in hydrogenolysis of xylitol over Ru-(Mn-Al)O_X catalyst in two successive runs [1].

Run	Activity [h^{-1}]	Carbon Selectivity [2] [%]							CB_T [4] [%]
		EG	PG	GLY	LA	C_4 Products [3]	C_5 Alditols	Gas Phase Products	
1	26	20	25	12	1	8	3	10	85
2	17	16	24	10	1	12	5	15	83

[1] Conditions: xylitol 1.0 wt % (1.5 g), 135 mL H_2O, 0.5 g catalyst (molar ratio xylitol/Ru: 77), 60 bar H_2, 200 °C; [2] determined at 80% conversion; [3] C_4 products: threitol, erythritol, butanediols; [4] CB_T: Total carbon balance.

Indeed, the activity only decreased from 26 to 17 h^{-1}, while the cumulated selectivity to GLY and glycols was 50% instead of 57%. The selectivity to C_4 and C_5 alditols increased slightly from 11% to 17% and the selectivity to gaseous products increased from 10% to 15%. Therefore, the recycling of catalyst favored the epimerization and cascade decarbonylation reactions and the Mn leaching after the second run was less than 2.0 wt % (55 mg L^{-1} in the final mixture). The XRD analysis of the reactivated catalyst (after 2nd run, Figure 7) revealed that the proportion of Mn_3O_4 in the crystalline bulk and amorphous phase had increased. These results showed that the structure of Ru-(Mn-Al)O_X catalyst was slightly altered under these hydrothermal conditions. After a reactivation under H_2, the selectivity to GLY and glycols remained at a good level.

3. Experimental Section

3.1. Materials

D-Xylitol (99%) and titanium isopropoxide (>99% after distillation) were purchased from Sigma Aldrich (St. Quentin Fallavier, France); Ru(NO)$(NO_3)_3 \cdot x H_2O$ (Ru > 31.3 wt %), $Al(NO_3)_3$,$9H_2O$ (>99%), $Mn(OAc)_2$ and Na_2CO_3 (>99%) from Alfa Aesar (Karlsruhe, Germany); $Mn(NO_3)_2 \cdot 4H_2O$ (98%) from Merck (Fontenay sous Bois, France); $Zn(NO_3)_2$,$6H_2O$ (99%) from AppliChem (Darmstadt, Germany); and $ZrO(NO_3)_2$,H_2O (99%) from Strem Chemical (Bischheim, France). Hydrogen (H_2 > 99.5%), argon (Ar > 99.5%), 1% *v*/*v* O_2/N_2, 1% *v*/*v* NH_3/He and 5% *v*/*v* CO_2/He gases were from Air Liquide (Paris, France).

3.2. Catalysts Preparation

The Ru-mixed oxide based catalysts were prepared by a standard co-precipitation method according to the literature [24,26]. In the synthesis of Ru-(Mn-Al)O_X catalyst, an aqueous solution (330 mL) of $Mn(NO_3)_2 \cdot 4H_2O$ (9.1 g), $Al(NO_3)_3 \cdot 9H_2O$ (3.4 g) and Ru(NO)$(NO_3)_3 \cdot x H_2O$ (0.4 g) and an aqueous solution (264 mL) of NaOH (10.5 g) and Na_2CO_3 (8.7 g) were added simultaneously dropwise under vigorous stirring at RT into a round-bottom 1 L flask and the pH was controlled at 12 ± 0.5. The obtained slurry was aged for 20 h at 80 °C, filtered, and washed a couple of times with hot deionized water (70 °C) until pH 7. Then, the cake was dried at 100 °C overnight, calcined under air flow (100 mL min^{-1}) at 460 °C for 2 h (3 °C min^{-1}) and reduced under H_2 flow (100 mL min^{-1}) for 3 h, and finally passivated under 1% O_2/N_2 gas mixture flow at RT for

30 min. The Ru-(Mn-Zr)O_X and Ru-(Mn-Zn)O_X catalysts were prepared analogously to this procedure. The Ru-(Mn-Ti)O_X was prepared as previously, however, $Mn(OAc)_2$ was used as the precursor due to the use of $Ti(OiPr)_4$ precursor. A support (Mn-Al)O_X was prepared by co-precipitation of $Mn(NO_3)_2{\cdot}4H_2O$ and $Al(NO_3)_3{\cdot}9H_2O$, according to the literature [24,26]. The material was dried and calcined, as previously. Ru/(Mn-Al)O_X catalyst was then synthetized by wet impregnation of the aqueous solution of Ru precursor over (Mn-Al)O_X, followed by reduction and passivation, according to the previous procedure [25].

3.3. Catalysts Characterization

The metal loadings of the investigated catalysts were determined after mineralization of the solids in aqua regia at 150 °C for 12 h and in aqueous HF, and analysis by inductively coupled plasma-optical emission spectroscopy (ICP-OES, Activa Jobin-Yvon). Powder X-ray patterns were recorded using a Brucker D8A25 diffractometer with CuK_α radiation and equipped with a multi-channel fast detector LynxEye over the range $10° < 2\theta < 80°$ at $0.02° \ s^{-1}$. The crystalline phases were identified using the JCPDS reference standards: $MnCO_3$ (44-1472), MnO (05-4310), $Mn(OH)_2$ (73-1604), Mn_3O_4 (06-6593), Mn_5O_8 (07-1171), Ru (06-0663). The crystallite sizes were calculated based on LVol-IB (d = 4/3 * LVol-IB) obtained by Rietveld refinement using Topas 5 software. The specific surface areas were determined by N_2 physisorption (ASAP 2020) at −196 °C after thermal outgassing (350 °C for 7 h under vacuum 10^{-4} mbar). The amount of basic and acidic sites on the catalyst surface were determined by temperature-programmed desorption (TPD, Belcat-M) of the probe CO_2 and NH_3, respectively, according to the procedure described previously [25]. The TEM images of replica were taken using a JEOL 2010 instrument operated at 200 keV.

3.4. Catalytic Testing

Hydrogenolysis of xylitol was carried out in a Hastelloy Parr autoclave (300 mL) at a stirring speed of 1000 rpm. In a typical run, 135 mL of 10 wt % xylitol aqueous solution and 0.5 g catalyst were introduced into the autoclave. After purging with Ar, the reactor was heated to the reaction temperature. It was then pressurized with H_2, which corresponded to the reaction time t = 0.

The products in the liquid samples were identified and quantified using two different HPLC instruments (Shimadzu, Marne la Vallée, France) connected to refractive index diffraction (RID10A) and UV detectors (SPD-M10A), as described previously [10]. The total organic carbon (TOC) in the liquid phase was measured using a TOC analyzer (Shimadzu TOC-VCHS equipped with ASI-automatic sampler) and compared to initial TOC to estimate the formation of products transferred to the gaseous phase. The carbon balance BC_T was determined by comparison of TOC measured and TOC calculated from HPLC. Conversion, selectivity (on a carbon basis %), and initial reaction activity ($mol_{xylitol}$ $mol_{Ru}{}^{-1}$ h^{-1}) were calculated as previously [10]. The metal leaching of the catalyst was detected by ICP-OES analysis of the final reaction medium.

4. Conclusions

To conclude, the Ru-(Mn-M)O_X (M: Ti, Al, Zr) catalysts displayed high performances in the valorization of xylitol under base-free conditions. Interestingly, due to the high number of basic sites, the catalysts were able to selectively produce glycols and glycerol with a very low amount of carboxylic acids, such as lactic acid. The Ru-(Mn-Al)O_X catalyst presented the highest activity ($57 \ h^{-1}$) and high cumulated selectivity (58%) to glycols and glycerol. That makes Ru-(MnO-Al)O_X one of the most selective Ru-based catalysts under these conditions. The comparison of Ru/(Mn-Al)O_X and Ru-(Mn-Al)O_X catalysts revealed that Ru/(Mn-Al)O_X was more active ($111 \ h^{-1}$), however, it produced more C_5-C_4 alditols as well as gas phase products (i.e., CH_4, C_2H_6). The reason is the smaller Ru particles observed by XRD and TEM, which favor decarbonylation, epimerization as well as cascade decarbonylation reactions. However, Ru-(Mn-Al)O_X catalyst was not stable during the reaction since 42 wt % of Mn-leaching and $MnCO_3$ phase were detected after reaction. The amount of catalyst in

the system has a strong effect on the catalyst performance. The Ru-(Mn-Al)O_X activity increased up to 101 h^{-1} as the molar ratio xylitol/Ru was decreased from 764 to 255. Moreover, the decrease in Mn-leaching allowed us to perform a recycling test. After catalyst reactivation, low deactivation was observed in the second run. Therefore, under the appropriate reaction conditions, Ru-(Mn-Al)O_X is a promising catalyst for the synthesis of glycols and glycerol from biomass-derived alditols.

Author Contributions: Funding acquisition, M.R.; Supervision, N.P., D.D., A.C., C.P. and M.B.; Writing—original draft, M.R. and M.B.; Writing—review & editing, N.P. and M.B.

Funding: This work was funded by Ecole Doctorale de Chimie de Lyon and IFP Energies Nouvelles.

Acknowledgments: The scientific platform of IRCELYON (Pascale Mascunan, Yoann Aizac, Laurence Burel) are acknowledged for ICP, XRD, and TEM analysis of the catalysts.

Conflicts of Interest: The authors declare no conflict of interest.

Appendix A

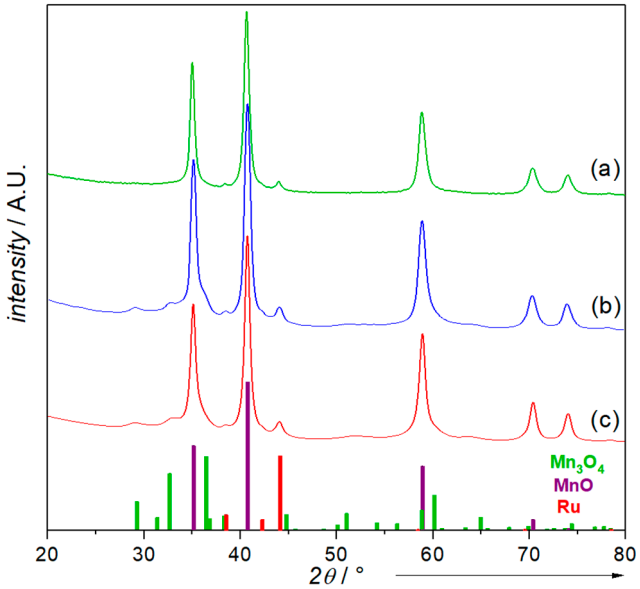

Figure A1. XRD patterns of Ru-(Mn-Al)O_X catalyst: (**a**) 4.0 s/step of 0.02°. (**b**) 16.0 s/step of 0.04°. (**c**) Simulated pattern obtained after Rietveld refinement with TOPAS software.

References

1. Yue, H.; Zhao, Y.; Ma, X.; Gong, J. Ethylene glycol: Properties, synthesis, and applications. *Chem. Soc. Rev.* **2012**, *41*, 4218–4244. [CrossRef] [PubMed]
2. Dasari, M.A.; Kiatsimkul, P.-P.; Sutterlin, W.R.; Suppes, G.J. Low-pressure hydrogenolysis of glycerol to propylene glycol. *Appl. Catal. A Gen.* **2005**, *281*, 225–231. [CrossRef]
3. Zheng, M.; Pang, J.; Sun, R.; Wang, A.; Zhang, T. Selectivity control for cellulose to diols: Dancing on the eggs. *ACS Catal.* **2017**, *7*, 1939–1954. [CrossRef]
4. Climent, M.J.; Corma, A.; Iborra, S. Converting carbohydrates to bulk chemicals and fine chemicals over heterogeneous catalysts. *Green Chem.* **2011**, *13*, 520–540. [CrossRef]
5. Besson, M.; Gallezot, P.; Pinel, C. Conversion of biomass into chemicals over metal catalysts. *Chem. Rev.* **2014**, *114*, 1827–1870. [CrossRef] [PubMed]
6. Ruppert, A.M.; Weinberg, K.; Palkovits, R. Hydrogenolysis goes bio: From carbohydrates and sugar alcohols to platform chemicals. *Angew. Chem. Int. Ed. Engl.* **2012**, *51*, 2564–2601. [CrossRef] [PubMed]
7. Jin, X.; Thapa, P.S.; Subramaniam, B.; Chaudhari, R.V. Kinetic Modeling of Sorbitol Hydrogenolysis over Bimetallic RuRe/C Catalyst. *ACS Sustain. Chem. Eng.* **2016**, *4*, 6037–6047. [CrossRef]

8. Hausoul, P.J.C.; Beine, A.K.; Neghadar, L.; Palkovits, R. Kinetics study of the Ru/C-catalysed hydrogenolysis of polyols—Insight into the interactions with the metal surface. *Catal. Sci. Technol.* **2017**, *7*, 56–63. [CrossRef]
9. Sun, J.; Liu, H. Selective hydrogenolysis of biomass-derived xylitol to ethylene glycol and propylene glycol on supported Ru catalysts. *Green Chem.* **2011**, *13*, 135–142. [CrossRef]
10. Rivière, M.; Perret, N.; Cabiac, A.; Delcroix, D.; Pinel, C.; Besson, M. Xylitol Hydrogenolysis over Ruthenium-Based Catalysts: Effect of Alkaline Promoters and Basic Oxide-Modified Catalysts. *ChemCatChem* **2017**, *9*, 2145–2159. [CrossRef]
11. Deutsch, K.L.; Lahr, D.G.; Shanks, B.H. Probing the ruthenium-catalyzed higher polyol hydrogenolysis reaction through the use of stereoisomers. *Green Chem.* **2012**, *14*, 1635–1642. [CrossRef]
12. Hausoul, P.J.C.; Negahdar, L.; Schute, K.; Palkovits, R. Unravelling the Ru-Catalyzed Hydrogenolysis of Biomass-Based Polyols under Neutral and Acidic Conditions. *ChemSusChem* **2015**, *8*, 3323–3330. [CrossRef] [PubMed]
13. Huang, Z.; Chen, J.; Jia, Y.; Liu, H.; Xia, C.; Liu, H. Selective hydrogenolysis of xylitol to ethylene glycol and propylene glycol over copper catalysts. *Appl. Catal. B Environ.* **2014**, *147*, 377–386. [CrossRef]
14. Banu, M.; Sivasanker, S.; Sankaranarayanan, T.M.; Venuvanalingam, P. Hydrogenolysis of sorbitol over Ni and Pt loaded on NaY. *Catal. Commun.* **2011**, *12*, 673–677. [CrossRef]
15. Liu, H.H.; Huang, Z.; Kang, H.; Li, X.; Xia, C.; Chen, J.; Liu, H.H. Efficient bimetallic NiCu-SiO_2 catalysts for selective hydrogenolysis of xylitol to ethylene glycol and propylene glycol. *Appl. Catal. B Environ.* **2018**, *220*, 251–263. [CrossRef]
16. Zhao, L.; Zhou, J.H.; Sui, Z.J.; Zhou, X.G. Hydrogenolysis of sorbitol to glycols over carbon nanofiber supported ruthenium catalyst. *Chem. Eng. Sci.* **2010**, *65*, 30–35. [CrossRef]
17. Guo, X.; Dong, H.; Li, B.; Dong, L.; Mu, X.; Chen, X. Influence of the functional groups of multiwalled carbon nanotubes on performance of Ru catalysts in sorbitol hydrogenolysis to glycols. *J. Mol. Catal. A Chem.* **2016**. [CrossRef]
18. Beine, A.K.; Krüger, A.J.D.; Artz, J.; Weidenthaler, C.; Glotzbach, C.; Hausoul, P.J.C.; Palkovits, R. Selective production of glycols from xylitol over Ru on covalent triazine frameworks—Suppressing decarbonylation reactions. *Green Chem.* **2018**, *20*, 1316–1322. [CrossRef]
19. Chen, X.; Wang, X.; Yao, S.; Mu, X. Hydrogenolysis of biomass-derived sorbitol to glycols and glycerol over Ni-MgO catalysts. *Catal. Commun.* **2013**, *39*, 86–89. [CrossRef]
20. Vijaya Shanthi, R.; Sankaranarayanan, T.M.; Mahalakshmy, R.; Sivasanker, S. Fly ash based Ni catalyst for conversion of sorbitol into glycols. *J. Environ. Chem. Eng.* **2015**, *3*, 1752–1757. [CrossRef]
21. Jin, X.; Shen, J.; Yan, W.; Zhao, M.; Thapa, P.S.; Subramaniam, B.; Chaudhari, R.V. Sorbitol Hydrogenolysis over Hybrid Cu/CaO-Al_2O_3 Catalysts: Tunable Activity and Selectivity with Solid Base Incorporation. *ACS Catal.* **2015**, *5*, 6545–6558. [CrossRef]
22. Murillo Leo, I.; López Granados, M.; Fierro, J.L.G.; Mariscal, R. Selective conversion of sorbitol to glycols and stability of nickel–ruthenium supported on calcium hydroxide catalysts. *Appl. Catal. B Environ.* **2016**, *185*, 141–149. [CrossRef]
23. Vijaya Shanthi, R.; Mahalakshmy, R.; Thirunavukkarasu, K.; Sivasanker, S. Hydrogenolysis of sorbitol over Ni supported on Ca- and Ca(Sr)-hydroxyapatites. *Mol. Catal.* **2018**, *451*, 170–177. [CrossRef]
24. Du, W.C.; Zheng, L.P.; Shi, J.J.; Xia, S.X.; Hou, Z.Y. Production of C2 and C3 polyols from D-sorbitol over hydrotalcite-like compounds mediated bi-functional Ni-Mg-Al-Ox catalysts. *Fuel Process. Technol.* **2015**, *139*, 86–90. [CrossRef]
25. Rivière, M.; Perret, N.; Delcroix, D.; Cabiac, A.; Pinel, C.; Besson, M. Solvent Effect in Hydrogenolysis of Xylitol over Bifunctional Ru/MnO/C Catalysts under Alkaline-Free Conditions. *ACS Sustain. Chem. Eng.* **2018**, *6*, 4076–4085. [CrossRef]
26. Neaţu, F.; Petrea, N.; Petre, R.; Somoghi, V.; Florea, M.; Parvulescu, V.I. Oxidation of 5-hydroxymethyl furfural to 2,5-diformylfuran in aqueous media over heterogeneous manganese based catalysts. *Catal. Today* **2016**, *278*, 66–73. [CrossRef]
27. Jeong, D.; Jin, K.; Jerng, S.E.; Seo, H.; Kim, D.; Nahm, S.H.; Kim, S.H.; Nam, K.T. Mn_5O_8 Nanoparticles as Efficient Water Oxidation Catalysts at Neutral pH. *ACS Catal.* **2015**, *5*, 4624–4628. [CrossRef]
28. Hem, J. *Chemical Equilibria and Rates of Manganese Oxidation*; Water-Supply Paper 1667-A; United States Government Publishing Office: Washington, DC, USA, 1963. [CrossRef]

29. Robinson, D.M.; Go, Y.B.; Mui, M.; Gardner, G.; Zhang, Z.; Mastrogiovanni, D.; Garfunkel, E.; Li, J.; Greenblatt, M.; Dismukes, G.C. Photochemical Water Oxidation by Crystalline Polymorphs of Manganese Oxides: Structural Requirements for Catalysis. *J. Am. Chem. Soc.* **2013**, *135*, 3494–3501. [CrossRef] [PubMed]
30. Gao, T.; Norby, P.; Krumeich, F.; Okamoto, H.; Nesper, R.; Fjellvåg, H. Synthesis and Properties of Layered-Structured Mn_5O_8 Nanorods. *J. Phys. Chem. C* **2010**, *114*, 922–928. [CrossRef]
31. Rekha, V.; Raju, N.; Sumana, C.; Paul Douglas, S.; Lingaiah, N. Selective Hydrogenolysis of Glycerol Over Cu-ZrO_2-MgO Catalysts. *Catal. Lett.* **2016**, *146*, 1487–1496. [CrossRef]
32. Mazzieri, V.; Coloma-Pascual, F.; Arcoya, A.; L'Argentière, P.C.; Figoli, N.S. XPS, FTIR and TPR characterization of Ru/Al_2O_3 catalysts. *Appl. Surf. Sci.* **2003**, *210*, 222–230. [CrossRef]
33. Ishikawa, M.; Tamura, M.; Nakagawa, Y.; Tomishige, K. Demethoxylation of guaiacol and methoxybenzenes over carbon-supported Ru–Mn catalyst. *Appl. Catal. B Environ.* **2016**, *182*, 193–203. [CrossRef]
34. Watanabe, M.; Aizawa, Y.; Iida, T.; Nishimura, R.; Inomata, H. Catalytic glucose and fructose conversions with TiO_2 and ZrO_2 in water at 473K: Relationship between reactivity and acid–base property determined by TPD measurement. *Appl. Catal. A Gen.* **2005**, *295*, 150–156. [CrossRef]
35. Bancquart, S.; Vanhove, C.; Pouilloux, Y.; Barrault, J. Glycerol transesterification with methyl stearate over solid basic catalysts: I. Relationship between activity and basicity. *Appl. Catal. A Gen.* **2001**, *218*, 1–11. [CrossRef]
36. Tajvidi, K.; Hausoul, P.J.C.; Palkovits, R. Hydrogenolysis of cellulose over Cu-based catalysts-analysis of the reaction network. *ChemSusChem* **2014**, *7*, 1311–1317. [CrossRef] [PubMed]
37. Zhou, Z.; Li, X.; Zeng, T.; Hong, W.; Cheng, Z.; Yuan, W. Kinetics of Hydrogenolysis of Glycerol to Propylene Glycol over Cu-ZnO-Al_2O_3 Catalysts. *Chin. J. Chem. Eng.* **2010**, *18*, 384–390. [CrossRef]
38. Hirano, Y.; Sagata, K.; Kita, Y. Selective transformation of glucose into propylene glycol on Ru/C catalysts combined with ZnO under low hydrogen pressures. *Appl. Catal. A Gen.* **2015**, *502*, 1–7. [CrossRef]
39. Sun, J.; Liu, H. Selective hydrogenolysis of biomass-derived xylitol to ethylene glycol and propylene glycol on Ni/C and basic oxide-promoted Ni/C catalysts. *Catal. Today* **2014**, *234*, 75–82. [CrossRef]
40. Ketchie, W.C.; Maris, E.P.; Davis, R.J. In-situ X-ray Absorption Spectroscopy of Supported Ru Catalysts in the Aqueous Phase. *Chem. Mater.* **2007**, *19*, 3406–3411. [CrossRef]
41. Trinh, T.-K.-H.; de Hemptinne, J.-C.; Lugo, R.; Ferrando, N.; Passarello, J.-P. Hydrogen Solubility in Hydrocarbon and Oxygenated Organic Compounds. *J. Chem. Eng. Data* **2016**, *61*, 19–34. [CrossRef]
42. Hu, C.-C.; Wu, Y.-T.; Chang, K.-H. Low-Temperature Hydrothermal Synthesis of Mn_3O_4 and MnOOH Single Crystals: Determinant Influence of Oxidants. *Chem. Mater.* **2008**, *20*, 2890–2894. [CrossRef]
43. Menezes, P.W.; Indra, A.; Littlewood, P.; Schwarze, M.; Göbel, C.; Schomäcker, R.; Driess, M. Nanostructured manganese oxides as highly active water oxidation catalysts: A boost from manganese precursor chemistry. *ChemSusChem* **2014**, *7*, 2202–2211. [CrossRef] [PubMed]